Journal of Membrane Science 672 (2023) 121423

Contents lists available at ScienceDirect

Journal of Membrane Science

journal homepage: www.elsevier.com/locate/memsci

Advanced ceramics in radical filtration: TiO_2 layer thickness effect on the photocatalytic membrane performance

Shuyana A. Heredia Deba [a,b], Bas A. Wols [a,c], Doekle R. Yntema [a], Rob G.H. Lammertink [b,*]

[a] Wetsus European Center of Excellence for Sustainable Water Technology, 8911 MA Leeuwarden, The Netherlands
[b] Membrane Science and Technology, Faculty of Science and Technology (TNW), University of Twente, Drienerlolaan 5, 7522 NB Enschede, The Netherlands
[c] KWR Water Research Institute, 3430 BB, Nieuwegein, The Netherlands

ARTICLE INFO

Keywords:
Photocatalytic membrane
Transport and reaction inside the membrane
Photocatalytic layer thickness
TiO_2 top layer

ABSTRACT

Membranes with advanced oxidation processes (AOPs) are a promising combination to separate and degrade organic pollutants in a single system. In this work, we describe the fabrication and characteristics of nine membranes with different TiO_2 top layer thicknesses (from 0.26 to 21.9 μm), giving attention to the critical catalyst thickness and the formation of defects. We also report the optimum photocatalyst thickness for our single-layer membranes (~2.74 μm), after which more titanium dioxide does not improve the degradation. However, an increase in degradation for membranes with multiple TiO_2 layers was still possible. These results and the comparisons with the literature suggested that the optimal catalyst thickness is closely related to the material morphology. We obtained a maximum degradation at the lower filtration rate (1.6 L m^{-2} h^{-1}) of 72% with a single layer membrane of 3.4 μm and 82% with a membrane with six layers of 21.9 μm. Furthermore, a 1D mass transport and reaction model that describes the coating thickness effect was developed and fitted with the experimental data. Other parameters are also discussed, such as light penetration limitations, surface area, and surface reaction rate constant. These results and analysis provide a better understanding of the fabrication and optimization of photocatalytic membranes.

1. Introduction

Membranes have gained an important place in chemical technology and are used in a broad range of applications [1]. However, when membranes are used in treatment processes, the separated phase becomes a secondary waste that needs additional treatment. The combination of membranes with advanced oxidation processes (AOPs) could separate and degrade organics pollutants in a single system. In such hybrid processes, chemical degradation and membrane retention can potentially be synergistic.

AOPs produce in situ transitory species (mainly hydroxyl radicals), which degrade toxic and refractory pollutants into water, carbon dioxide, and mineral acids or into other more innocuous products. Besides, the partial decomposition of non-biodegradable organic pollutants can lead to biodegradable intermediates [2]. As such, AOP provides an attractive method for degrading persistent contaminations from water sources.

Among AOPs, photocatalytic oxidation with titanium dioxide has received particular attention as it is a common semiconductor, chemically and thermally stable, non-toxic, inexpensive, environmentally friendly, and commercially available [3]. A photocatalytic top layer in a membrane will help to degrade the retained organic molecules keeping the advantage typical in membrane processes of no addition of chemicals in the feed stream. Moreover, the photocatalytic activity can reduce membrane fouling, increasing the filtration performance and life span of the membrane and reducing replacement costs [4–7].

Depositing the photocatalytic coating onto a ceramic membrane presents a promising combination for industrial applications since ceramic membranes have outstanding features over polymeric membranes. Thanks to their chemical, thermal and mechanical properties, they can withstand more cleaning processes (i.e., backwash, harsh cleaning agents, or high temperatures) and offer reliable performance over long periods [8].

Several challenges are still to be solved to implement the use of photocatalytic membranes, such as mass transfer limitations, the nature of the intermediate products during the degradation, catalysis deactivation, photon transfer limitations, or low quantum efficiency, among others [9,10]. Various research efforts have been addressed to modify the TiO_2 structural and electronic properties to absorb light at larger wavelengths in the solar radiation spectrum by band gap engineering [11], thereby improving the quantum efficiency and photon transfer

* Corresponding author.
E-mail address: r.g.h.lammertink@utwente.nl (R.G.H. Lammertink).

https://doi.org/10.1016/j.memsci.2023.121423
Received 17 November 2022; Received in revised form 19 January 2023; Accepted 22 January 2023
Available online 24 January 2023

limitations. Another optimization concerns the best catalyst load. In configurations with the photocatalyst in slurry, excessive amounts of TiO_2 hinder the penetration of UV light and hence worsen the degradation process. Meanwhile, in systems with the TiO_2 immobilized, the optimum catalyst load is characterized by the coating thickness with the best performance. A larger thickness will contain more catalyst but does not necessarily translate into better degradation when light penetration is limited. This parameter is closely related to the diffusion of the reactants to the active catalyst sites.

Light penetration, surface area, and pore connectivity inside the photocatalytic layer are essential to determine the optimal catalyst thickness. Different optimum coated catalyst thicknesses have been reported in literature. Rafieian et al. [12] reported an optimal thickness of 50 nm for magnetron sputtered TiO_2 films coated on silicon wafers. They worked with dense anatase layers from 9 nm to 0.5 μm. The density of the film could explain why there is not much difference in the membrane performance when increasing the thickness since the available surface area is not affected by this. Dundar et al. [13] studied TiO_2 thin films in the thickness range of 50 to ca. 800 nm deposited by ultrasonic spray pyrolysis and reported the highest photocatalytic activity in the range of 170–230 nm thick films during the degradation of stearic acid. The optimal thickness is higher than in the previous example possibly due to the formation of pinholes or a nonuniform coverage on the substrate by the TiO_2 deposited films. Visan et al. [14] reported an optimal thickness at 2.0 μm for a porous TiO_2 layer immobilized on silicon wafers. They fabricated homogeneous layers by spin-coating with thicknesses from 0.31 to 1.2 μm by changing the dispersion solution solid amount and by adding multiple layers to get thicknesses up to 4 μm. The layer porosity was 45% , and no defects were reported on the surface of the films. High porosity enhances the surface area reached by the UV light [15]. Phan et al. [16] found an even larger optimal catalyst thickness, 15 μm, in a fixed-bed photocatalytic membrane reactor in a dead-end cell supported by a polyamide membrane. They formed a cake from 2.5 to 20 μm thickness on top of the membrane with a uniform TiO_2 dispersion (250 nm average particle size). This large optimal catalyst thickness could be explained by multireflection and interconnection effects present in the cake structure [17]. These results show the dependency of the optimal catalyst thickness with the material morphology (porosity and pore size).

In the past years, various studies have been carried out to describe the photocatalytic degradation of micropollutants, and current models studying photocatalytic membranes [16,18] exclude the role of the membrane since the membrane is included only as a support. There is a need for more fundamental engineering science models that integrate photocatalytic oxidation and membrane technology [19]. In our previous work [20], a simple analytic 1D transport and surface reaction model was provided, which includes the membrane function (retention) and the photocatalytic oxidation (reaction). We related the transport phenomena and the photocatalytic reaction on the membrane surface, but the influence of the membrane thickness was not considered.

The objective of the present work is to study the effect of coated catalyst thickness and present a model that is able to explain this effect. Nine photocatalytic nanofiltration ceramic membranes with thicknesses from 0.26 to 21.9 μm have been fabricated and evaluated. The function of these photocatalytic membranes was experimentally studied in a single-pass dead-end membrane reactor for the discoloration of methylene blue. A model that successfully describes these experimental results, including the implications of varying the photocatalytic layer thickness, is provided. This work adds valuable information to the photocatalysis field to improve the fabrication of photocatalytic ceramic membranes for different applications.

2. Materials and methods

2.1. Photocatalytic membranes fabrication

Nine photocatalytic membranes were fabricated and used for this study. α–Alumina supports (α–Al_2O_3, ø28 mm, 2 mm thick, and 80 nm pore size) were purchased from Pervatech B.V., The Netherlands. These ceramic substrates ensure the mechanical stability of the membranes under pressure. A single layer of γ–alumina (γ–Al_2O_3) was deposited on the polished side of the α–alumina supports by dip-coating it in a boehmite sol in a dust-free room. The α–alumina support was brought in contact with boehmite sol for 3 s and subsequently removed from the sol with an angular rate of 0.06 rad s^{-1}. This layer was then calcined in a temperature programmable furnace with an air atmosphere at 650 °C for 3 h. The gamma layer creates a smoother surface and improves the adhesion of the photocatalytic layer on top. Further details for the fabrication and the characteristics of the γ–Al_2O_3 layer can be found elsewhere [21–23]. The TiO_2 layer was formed on the γ–Al_2O_3 layer by the same dip-coating procedure and using a titanium dioxide suspension (Evonik, VP Disp. W 2730 X) with different concentrations (from 0.05 to 1.5 wt.%) depending on the desired thickness. The resulting layer was sintered for 2 h at 500 °C in the same furnace. The heating and cooling rates were kept at 2 °C min^{-1}. In the case of membranes with multiple TiO_2 layers, every additional layer was added after the thermal treatment process to improve the adhesion between layers. The membranes were cleaned after each experiment following the same thermal treatment. The membranes were stable under mechanical stress, but the TiO_2 layer could be removed by peeling with tape. The titanium dioxide crystalline structure of the top layer, a mixture of anatase and rutile, was reported in our previous work [20].

2.2. Membrane characterization

For the characterization of the membranes, high resolution SEM (Analysis Zeiss MERLIN HR-SEM) was used to investigate the morphology and cross-section. The pore size of the membranes was determined by permporometry using cyclohexane as condensing vapor. The experimental procedure is described in detail elsewhere [24].

Water permeability experiments were performed in a dead-end photocatalytic membrane reactor (PMR) by measuring the transmembrane pressure as a function of the water flux. All measurements were conducted in duplicate. The permeability was then calculated as the slope of the flux versus pressure difference over the membrane.

2.3. Photocatalytic degradation experiments

The nine fabricated membranes were tested regarding the photocatalytic dye degradation using an in-house built photocatalytic membrane reactor, see Heredia Deba et al. [20] for details on the set-up configuration and the PMR. Dead-end filtration and degradation experiments were carried out using methylene blue solution (MB) (BOOM, CAS 61-73-4), $C_{16}H_{18}ClN_3S$, as an azo-dye model compound. An aqueous solution of 4 mg L^{-1} of MB dissolved in water containing 1.0 mM sodium sulphate was pumped into the setup with fluxes of 1.6, 3.3, 6.5, 9.7, 13.0, and 16.2 L m^{-2} h^{-1}. These fluxes are in the range typically used in commercial nanofiltration. Sodium sulphate anhydrous (VWR chemicals, CAS 7757-82-6), Na_2SO_4, was used to avoid corrosion. The UV radiation was set to 210 W m^{-2} using a LED lamp (NCSU276AT) placed 67 mm away from the membrane surface, with an additional lens (AL-12M-119) to narrow the light distribution angle to 8 degrees. The experiments were repeated twice as the reproducibility of the experiments was found to be high. The natural pH of the system was used without further adjustment.

The discoloration of MB was continuously monitored by passing the permeate through an optical flow cell (FIA-Z-SMA-ML-PE flow

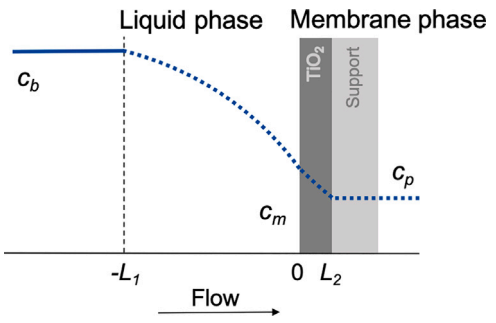

Fig. 1. Schematic representation of the 1D model, indicating the liquid phase, reservoir length L_1, membrane phase for three different catalyst thickness L_2, and concentration profile where c_b is the inlet concentration, c_m is the concentration on the membrane surface, and c_p is the permeate concentration.

cell, 10 mm path length) connected to a UV–Vis spectrometer (Flame Model Spectrometer with Sony Detector, Ocean Optics). The monitored wavelength, 664 nm, corresponds to the maximum absorption peak of MB. Prior to the experiment, the membranes were equilibrated for 2 h with the feed solution to account for any dye removal due to adsorption on the membrane surface. Then the LED was turned on, and the experiment was concluded when the outlet absorbance reached a steady value at each filtration rate. Additionally, control experiments were carried out with a membrane without the TiO_2 layer using the same average irradiation (210 W m^{-2}), and no significant removal of methylene blue was observed, even at the lowest permeation rate.

2.4. Mass transport and reaction model

In our previous paper [20], we describe a 1D transport and surface reaction model where the photocatalytic reaction takes place only on the membrane surface during a dead-end filtration. In a photocatalytic reaction, the photocatalyst absorbs photons to excite valence band electrons onto the conduction band, which results in highly active photo-generated holes (h^+) in the valence band and photo-generated electrons (e^-) in the conduction band [25,26]. The photo-generated h^+ and e^- can then diffuse to the TiO_2 surface to generate reactive oxygen active species (O_2^-, OH^-, H_2O_2, etc.), that can degrade organic molecules.

In the approach presented here, we consider the reaction inside the photocatalytic layer, based on a simplified kinetic expression that assumes the rate proportional to the MB concentration and UV light intensity. For this purpose, two regions are defined; the liquid phase in contact with the membrane (of thickness L_1) and the membrane phase (of thickness L_2). Both regions are included since there is no stirring in the system, and significant concentration gradients are expected in both phases. The concentration profile is solved for both regions on a $\tilde{z}_1 = [0, L_1]$ and $\tilde{z}_2 = [0, L_2]$, respectively, thereby effectively shifting the liquid domain from $[-L_1, 0]$ to $[0, L_1]$. Fig. 1 illustrates the schematics of the model.

Assuming only the perpendicular flow through the membrane, we obtain a steady state advection diffusion balance in the liquid region. In dimensionless form, it is given as:

$$\mathrm{Pe}_1 \frac{dc_1}{dz_1}\bigg|_{0<z_1<1} = \frac{d^2c_1}{dz_1^2} \tag{1}$$

while the second region, the porous membrane, will have advection, diffusion and reaction. The dimensionless expression is:

$$\mathrm{Pe}_2 \frac{dc_2}{dz_2}\bigg|_{0<z_2<1} = \frac{d^2c_2}{dz_2^2} - \frac{k' S_a \rho_c (1-\varepsilon) L_2^2}{D_2} c_2 \tag{2}$$

with dimensionless distance $z_i = \tilde{z}/L_i$, dimensionless concentration $c_i = \tilde{c}/c_b$, inlet concentration c_b [mg L^{-1}] and Péclet number, $\mathrm{Pe}_i = u_i L_i / D_i$, with linear velocity u_i [m s^{-1}], liquid reservoir height L_1 [m], membrane thickness L_2 [m] and diffusivity D_i [m^2 s^{-1}]. The reaction term further contains surface reaction rate constant k' [m s^{-1}], specific surface area S_a [9×10^4 m^2 kg^{-1}], catalyst density ρ_c [3895 kg m^{-3}], and porosity ε [0.45]. Note that this expression assumes a first-order reaction for the contaminant and that it is treated as an effective bulk reaction within the porous domain. k' includes the light absorption effect, as explained below.

As the internal boundary condition between liquid and membrane, assuming a constant cross-sectional area, we have: $u_2 = \frac{u_1}{\varepsilon}$, $c_2 = c_1 \alpha_r$, $D_2 = \varepsilon D_1 \left(1 + \frac{(u_2 r / D_1)^2}{48}\right)$. The latter is based on Taylor dispersion through pores of radius r, which is approximately 5 nm for these membranes, and the porosity effect ($\varepsilon = 0.45$) on diffusion. As we work with low velocities, we can safely assume $D_2 = \varepsilon D_1$. The intrinsic membrane retention 1-α_r is also considered to include the membrane function, where $\alpha_r = 1$ refers to no retention and $\alpha_r = 0$ to complete retention. Note that later we will analyze our data assuming no retention, $\alpha_r = 1$, as no retention was measured in the experiments with these membranes [27].

Considering k' as a depth-dependent reaction rate based on light absorption by the photocatalyst, it can be expressed as:

$$k'(z_2) = k'_0 \exp^{(-z_2 L_2 \alpha_p)} \tag{3}$$

where α_p [m^{-1}] is the UV light absorption coefficient of the photocatalyst. This expression thus describes the exponential decaying light intensity, with an accompanying reaction rate constant, through the photocatalytic layer.

As boundary conditions, firstly, we have a constant inlet concentration at z_1=0 for the liquid domain (for ease of using a positive velocity u),

$$c|_{z_1=0} = 1 \tag{4}$$

Secondly, we obtain the following flux continuity between the liquid ($z_1 = 1$) and membrane phase ($z_2 = 0$):

$$\varepsilon \left(c_1 - \frac{1}{\mathrm{Pe}_1}\frac{dc_1}{dz_1}\right)\bigg|_{z_1=1} = \left(c_2 - \frac{1}{\mathrm{Pe}_2}\frac{dc_2}{dz_2}\right)\bigg|_{z_2=0} \tag{5}$$

The final boundary condition concerns the outflow of the membrane phase. As Danckwerts postulated [28]:

$$\frac{dc_2}{dz_2}\bigg|_{z_2=1} = 0 \tag{6}$$

Inclusion of the surface reaction term at the boundary is also possible. Nevertheless, we observed that including this contribution does not have a significant influence when evaluating the permeate concentration for the k' range we obtained.

The permeate concentrations were experimentally obtained for nine membrane thicknesses, from 0.26 to 21.9 μm, for six filtration rates, from 1.6 to 16.2 L m^{-2} h^{-1}, with two repetitions per experiment. The k'_0 was fitted to the experimental results by solving the model in matlab using the bvp5c solver.

3. Results and discussion

3.1. Membrane characterization

SEM images were used to estimate the thickness of the layers and to compare the morphology and homogeneity of the γ–alumina interlayer and the TiO_2 top layers. Fig. 2 depicts SEM images of the thinner (image A) and thicker (image B) photocatalytic membranes with one layer of catalyst and the thicker membrane with multiple catalyst layers (image C) used in these experiments. The 0.26 ± 0.05 μm TiO_2 layer (image A) was obtained by dip-coating with a 0.05 wt% TiO_2 dispersion and the 4.3 ± 0.1 μm TiO_2 layer (image B) was obtained by dip-coating with a 1.50 wt% TiO_2 dispersion. Meanwhile, each of the six layers with a

Table 1
Membranes layer thickness and pore size.

TiO_2[a] [wt.%]	# layers	Pore diameter [nm]	Gamma layer thickness [μm]	TiO_2 layer thickness [μm]
0.05	1	5.8 ± 0.1	2.6 ± 0.1	0.26 ± 0.05
0.15	1	6.4 ± 0.1	2.33 ± 0.07	0.65 ± 0.04
0.30	1	5.8 ± 0.1	2.24 ± 0.08	1.17 ± 0.02
0.50	1	5.9 ± 0.1	1.72 ± 0.05	1.69 ± 0.04
0.70	1	6.5 ± 0.1	2.0 ± 0.2	2.74 ± 0.04
1.00	1	6.7 ± 0.1	2.2 ± 0.2	3.4 ± 0.1
1.50	1	5.9 ± 0.1	1.56 ± 0.07	4.3 ± 0.1
1.00	3	5.8 ± 0.1	1.25 ± 0.07	10.6 ± 0.1
1.00	6	6.7 ± 0.1	1.6 ± 0.2	21.9 ± 0.7

[a]TiO_2 content in the dispersion used for the dip-coating.

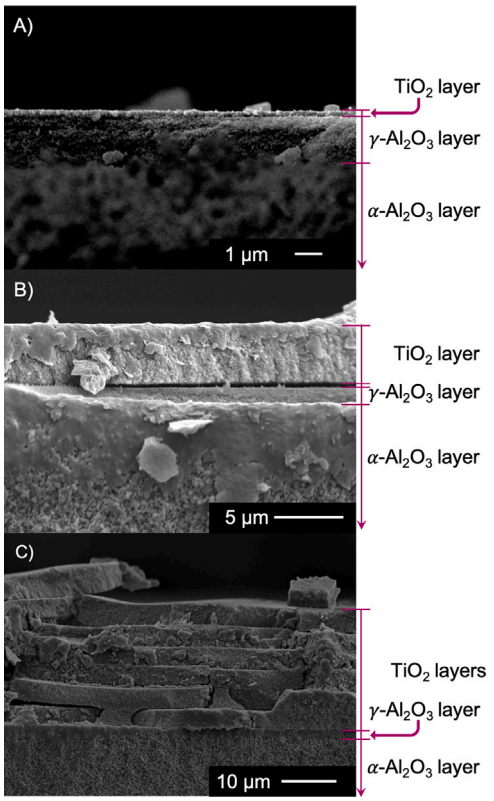

Fig. 2. Cross-sectional SEM images of three photocatalytic membranes. Image (A) presents a membrane with a very thin and homogeneous TiO_2 top layer obtained by dip-coating with a 0.05 wt.% TiO_2 dispersion, image (B) shows a membrane with a homogeneous TiO_2 top layer obtained by dip-coating with a 1.50 wt.% TiO_2 dispersion, and image (C) illustrates a membrane with six TiO_2 layers obtained by dip-coating six times with a 1.00 wt.% TiO_2 dispersion.

thickness of 3.6 ± 0.2 μm each (image C) was obtained by dip-coating with a 1.00 wt.% TiO_2 dispersion.

The three sections, α–alumina, γ–alumina, and TiO_2, are visible in Fig. 2. The thickness of the γ–alumina layer varies among ~1.5 or ~2.3 μm between membranes because the membranes were fabricated in different batches and the boehmite sol had a different concentration (between 0.5 and 0.6 M). We have not observed any difference in discoloration of methylene blue as a consequence of this variation in interlayer thickness. The membrane pore size characterization by permporometry showed mesopores between 5.5 and 6.9 nm, corresponding to the pore size of the γ–alumina layer. Table 1 summarizes the membrane layers thickness of all the membranes used in this investigation with the standard error obtained from several measurements from the same cross-section image and their pore sizes with the standard error of the technique.

It was not possible to form stable photocatalytic layers using concentrations of dispersion larger than 1.50 wt.% (resulting in 4.3 μm thickness, Fig. 2(B), as thicker layers delaminate from the membrane after sintering. Multiple coatings with a 1.00 wt.% dispersion with sintering in between were applied to increase the thickness beyond 4.3 μm. The membranes made with multiple TiO_2 layers were the most fragile as some small pieces of catalyst flaked off after the first experiment. Aguado et al. [29] hypothesized that the repulsion between layers with the same charge could cause a more open structure resulting in defects between the titania layers.

Fig. 3 reveals the top view of two photocatalytic membranes. Image (A) shows the surface of a photocatalytic membrane with three TiO_2 layers. This SEM picture was taken after the experiments, and it is visible that some pieces of catalyst have delaminated. In contrast, image (B) depicts a more homogeneous surface of a membrane with a single 1.69 μm thick TiO_2 top layer made with a 0.50 wt% dispersion.

It is common to observe layers cracking when the film thickness exceeds a certain critical thickness [30]. During the drying of the layers, the layer thickness is reduced, generating stress inside the film. Above a critical thickness, the energy required to extend the crack is lower than the energy gained from the relief of stress near the crack [31]. For our photocatalytic membranes, the critical thickness seems to be around 1.69 μm, as we observed cracks on the surface of membranes with layers above this thickness. For the sintering of these membranes, we used a heating rate of 2 °C min^{-1}. A lower rate could potentially reduce the stresses developed from the unequal thermal expansions coefficient of the support and the titania layer [32,33], but this has not been explored here.

Transmembrane pressure measurements showed that the pressure increases linearly with the pure water flux for all membranes. Fig. 4 presents the water permeability values obtained from the slope of the linear fit between the water flux and the pressure, with the standard error of the slope, for the α–alumina support, the support with the γ–alumina layer, and the membranes used in the experiments (logarithmic scale on top to identify the TiO_2 layer thickness). The water permeability obtained for the α–alumina support (4.96 ± 0.04 L m^{-2} h^{-1} bar^{-1}) is slightly reduced upon adding the γ–alumina layer. Although the α-alumina layer has much larger pore sizes (80 nm) compared to the γ-alumina layer, it is also much thicker, resulting in the dominating hydraulic resistance for this α-alumina layer. The TiO_2 layers are not adding any extra resistance, as their thicknesses are also limited.

Fig. 4 also shows the slight increase in permeability during the experiments with methylene blue. This is caused by the increase of temperature in the system by the UV light irradiation, which slightly reduces the solution viscosity. Nevertheless, the experiments are flow controlled, so the slight variation in permeability will only affect the transmembrane pressure, while the permeate flow rate is unaffected.

3.2. TiO_2 layer thickness effect on the discoloration of MB

Methylene blue discoloration experiments were conducted in a single-pass dead-end PMR under an average irradiation of 210 W m^{-2}.

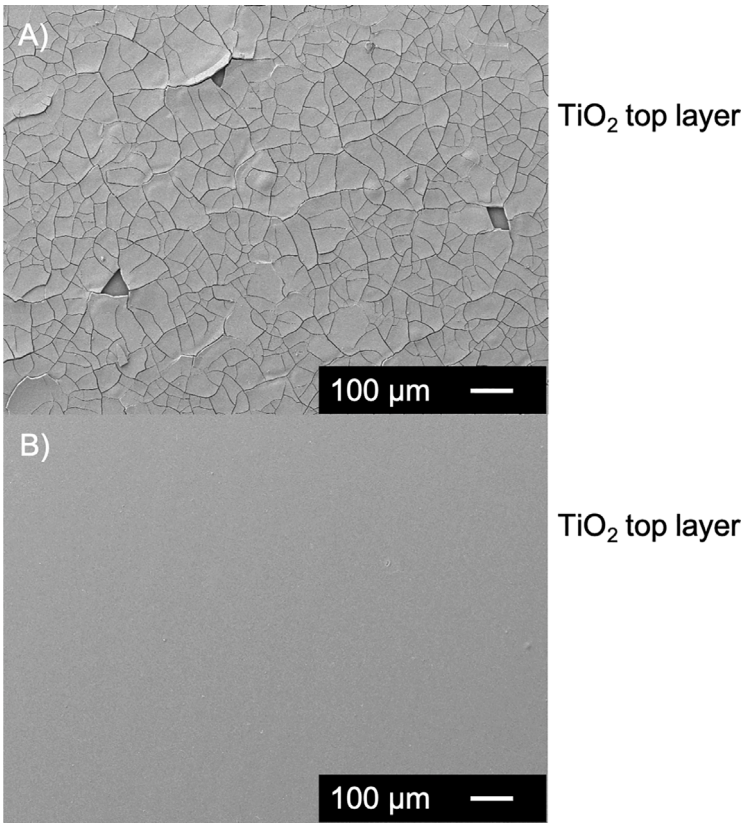

Fig. 3. Top SEM images of two photocatalytic membranes. Image (A) presents a membrane surface full of defects made with three TiO_2 layers obtained by dip-coating three times with a 1.00 wt% TiO_2 dispersion, and image (B) illustrates a smooth membrane surface fabricated with one TiO_2 layer obtained by dip-coating with a 0.50 wt% TiO_2 dispersion.

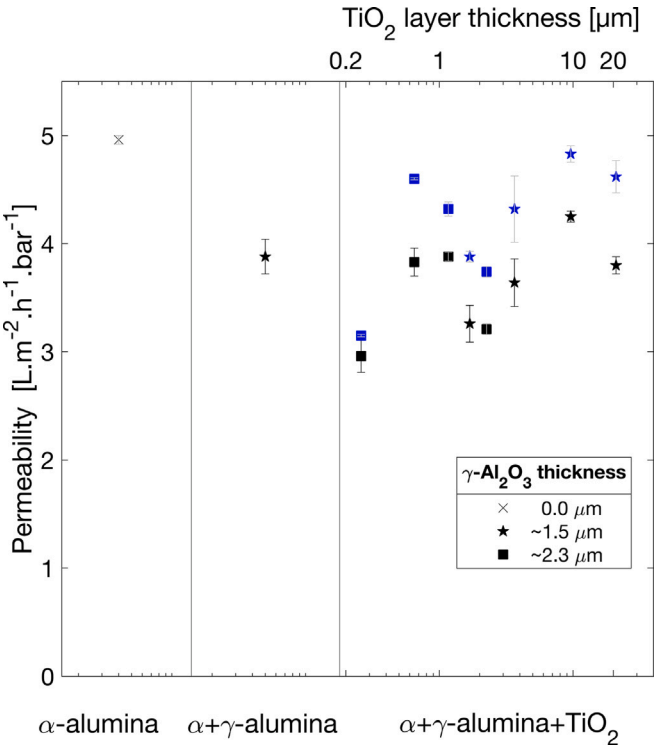

Fig. 4. Pure water permeability for the α-alumina support only, coated with γ-alumina, and subsequently coated with titania represented by symbols in black. Aqueous methylene blue solution permeability during the experiments with the photocatalytic membranes is depicted by symbols in blue.

Fig. 5 shows the MB normalized permeate concentration (c_p/c_b) for the lowest and highest filtration rate for different membrane thicknesses. A degree of discoloration of 53% was achieved with the thinner membrane (0.26 μm), and 81% for the thicker membrane (21.9 μm) at the lowest flow rate (1.6 L m^{-2} h^{-1}).

The discoloration of MB increased with the increase of photocatalytic layer thickness. The degradation seems to stabilize for thicknesses beyond the TiO_2 layer thickness of 2.74 μm for all the studied filtration rates without considering the multi-layers membranes. Surprisingly, the thicker membranes with multiple layers showed further improved degradation. The cracks on the surface and across the multiple layers may act as interconnected mesopore channels, which increase the density of active sites (i.e., larger surface area), promote the flux density used, and facilitate the diffusion of reactants and products. Furthermore, the cracks in the TiO_2 layers may allow multireflections inside the different layers, which could improve the UV light harvesting efficiency [17]. We will later discuss these observations using the mass transport and reaction model, in Section 3.4.

3.3. Photonic efficiency

The photonic efficiency or lower limit of the quantum yield assess the light utilization efficiency of a photoreactor. Fig. 6(a) shows the photonic efficiency as a function of the filtration rate and Fig. 6(b) depicts the photonic efficiency for the lowest and highest filtration rate for the different membrane thicknesses. The photonic efficiency was calculated by the relation between the discolored MB moles [mol s^{-1}] and the incident photon flux [2.02×10^{-7} mol s^{-1}, conversion for 366 nm: 1 W = $3.06 \cdot 10^{-6}$ mol s^{-1} [34]]. The obtained values represent a minimum photonic efficiency since only the discoloration of MB is considered instead of the formation of electron–hole pairs or reactive

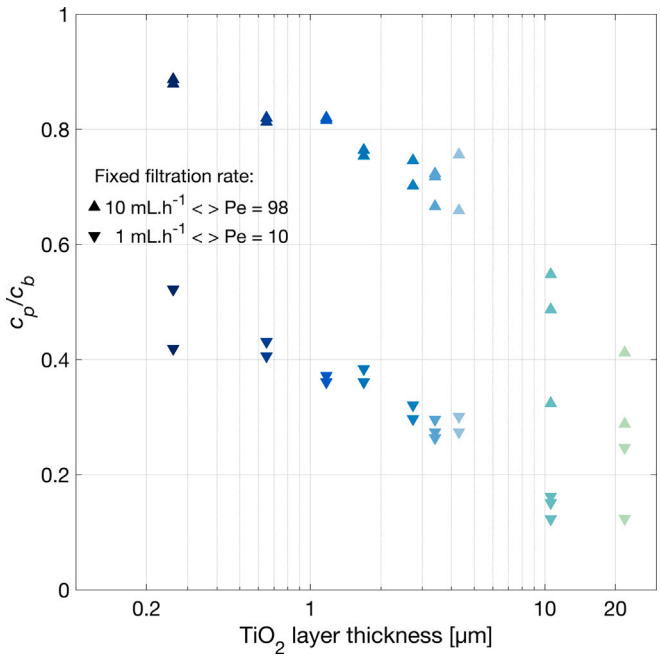

Fig. 5. Photocatalytic discoloration of methylene blue as a function of the catalytic layer thicknesses at the highest and lowest filtration rates.

oxygen species. The discoloration of MB is an indirect reaction with the incident photons since more reactions, that are not measured in these experiments, are possibly triggered by the photons. Researchers like Lizhogn et al. [35] calculated the quantum yield with the generation rate of hydroxide radicals.

Fig. 6(a) shows how the filtration rate affects the photonic efficiency. The improvement is a direct consequence of the increased transport rate towards the membrane at higher flow rates. As such, the photonic efficiency increases almost linearly with the filtration rate, except for the lower thicknesses, where it levels off at higher flows. As the thinnest membrane gives the lowest conversion, it is less influenced by mass transport limitations.

In Fig. 6(b), the photon efficiency is presented for different thicknesses of TiO_2. Thicker membranes show higher efficiencies since more photons can be absorbed. This effect is more substantial at higher flow rates due to earlier mentioned improved mass transport. We do expect a less than linear increase in photon efficiency with TiO_2 thickness, due to the light intensity decay within this layer.

The photonic efficiency can vary depending on the parameters used for its calculation, making it more difficult to compare with other systems. The reported values are not more than a few percent and depend on the photocatalyst and experimental conditions [36], e.g., 0.92% [37], 0.74% [38], or 0.09% [39] for the degradation of methylene blue over thin films of TiO_2, and 0.34% and 2.36% [40] for the MB degradation in a slurry configuration. The maximum photonic efficiency obtained in this work was only 0.012% for the thickest membrane (21.9 μm) with the highest flow rate (10 mL h^{-1}). The highest flowrate ensures the least mass transport limitation, while the thickest photocatalyst layer governs maximum absorption. The relatively low photonic efficiency may be caused by extensive reflection by the membrane surface, or other processes that limit the generation of reactive species.

3.4. Mass transport and reaction model

A model that predicts the permeate concentration by calculating the surface reaction constant has been described to analyze the reaction kinetics during the photocatalytic degradation of organic molecules by TiO_2 membranes with different thicknesses. Fig. 7(a) depicts the normalized MB permeate concentration (c_p/c_b) as a function of the filtration rate, where the lines represent the mass transport and surface reaction model fits and the symbols the experimental data. Fig. 7(b) illustrates the kinetic constant k_0' fitted to the experimental results with the error bars representing the nonlinear regression prediction confidence intervals.

The surface reaction rate constant k' is proportional to the local light intensity and follows an exponential decay with distance, see Eq. (3), according to Lambert–Beer law for light attenuation. This model accounts for the catalyst thickness variations and light absorption, and a unique k_0' can be obtained from fitting the experimental data for each thickness to the model. As expected from the analysis in Section 3.2, the membranes with a single coated top layer of TiO_2 behave differently than those with multiple layers. The performance of the seven membranes with one layer can be fitted to a single or averaged k_0' of $3.4 \pm 0.2 \times 10^{-8}$ m s^{-1} while the multi-layer membranes fit to $k_0' = 1.3 \pm 0.2 \times 10^{-7}$ m s^{-1} when the same absorption coefficient is considered during the fitting. The multi-layer membranes, thus, perform better than expected based on the single-layer performance. The absorption coefficient, $\alpha_r = 1.073 \times 10^6$ m^{-1}, of the TiO_2 layer has been experimentally measured before for titanium dioxide layers formed from the same dispersion [14], and we do not expect any differences for this between our layers.

Notably, in Fig. 7(a), the experimental data with the membrane with three layers (10.6 μm) show significant scatter between repetitions. After the first experiment with a multi-layer membrane, significant delamination was observed. In the case of the membrane with six layers, the first experiment was a permeability measurement which is why the reproducibility of the results is somewhat better. The multi-layer membranes show improved performance with high degradation but limitations regarding stability compared to single-layer membranes. Potential improvements could be obtained by further tuning the sintering temperature profile.

In Fig. 7(b), the model predictions for the thinnest membrane, 0.26 μm, differ a bit from the other membranes with one titanium dioxide top layer. The TiO_2 interaction with the alumina support could explain this reaction improvement. Alumina is an insulator that could trap photo-generated electrons and prevent their transfer from the TiO_2 particles to the interface with the fluid, influencing recombination rates and hence the photocatalytic activity. Egerton [41] measured lower photocatalytic activity when coating rutile particles with alumina or silica. They supported the idea that the coating blocks the transfer of both photo-generated holes and electrons by the reduction of photocatalytic oxidation and photocatalytic reduction. Gomez et al. [42] created coatings with a mixture of α–alumina and TiO_2. Their study concluded that the presence of Al_2O_3 decreases the electron–hole recombination as it acts as a charge transfer catalyst.

4. Conclusion

The influence of the catalyst coating thickness on a ceramic membrane has been studied for the photocatalytic discoloration of methylene blue. Nine membranes were fabricated by dip-coating alumina substrates in different TiO_2 dispersion concentrations or by increasing the number of layers. Cracks on the top layer were observed for membranes thicker than 1.69 μm (0.50 wt.% dispersion), and delamination occurred beyond 4.3 μm (1.50 wt.% dispersion). A 1D model was developed, which includes mass transfer, the surface reaction rate constant, and layer thickness on the overall discoloration of methylene blue. The model includes the effect of light absorption as a function of the depth in the photocatalyst layer. The obtained surface reaction rate constant illustrates that multiple layers provide enhanced reactivity compared to single catalytic layers, however, at the expense of layer stability. Furthermore, the thinnest membrane suggests a slight positive influence regarding reactivity, possibly based on the effect of the substrate

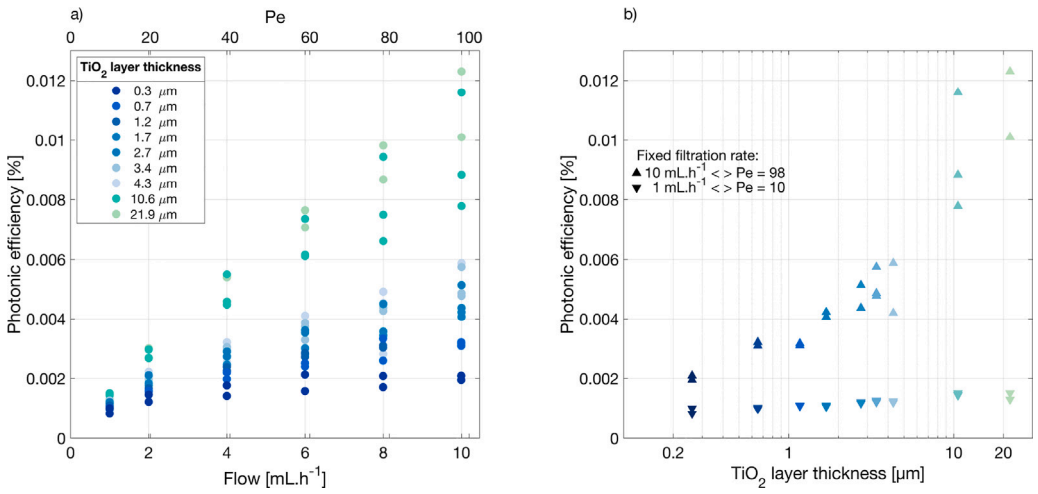

Fig. 6. Figure (a) shows the photonic efficiency as a function of the filtration rate. Figure (b) illustrates the photonic efficiency vs. membrane thickness at the highest and lowest filtration rates.

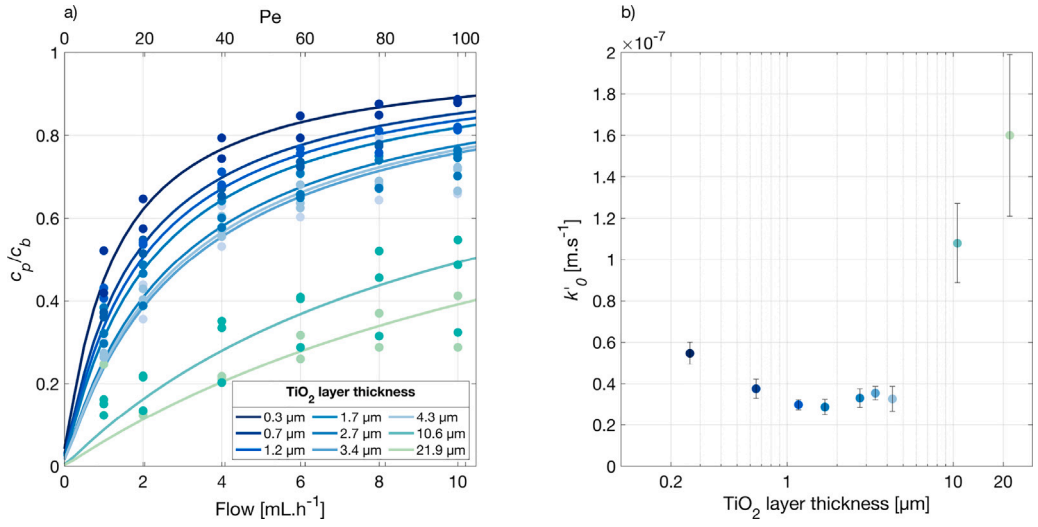

Fig. 7. Figure (a) shows the discoloration of MB vs. filtration rate. Symbols depict experimental results and lines correspond to the mass transport and surface reaction model. Figure (b) displays the fitted k_0' for different catalytic layer thicknesses.

on the recombination rate. This work provides valuable information in the fabrication of photocatalytic membranes and contributes with a model that includes the catalyst thickness effect on photocatalytic degradation. Undoubtedly, this knowledge will help in the promising use of membranes combined with advanced oxidation processes to exploit the synergy between both.

CRediT authorship contribution statement

Shuyana A. Heredia Deba: Formal analysis, Investigation, Methodology, Data curation, Visualization, Validation, Writing – original draft. **Bas A. Wols:** Software, Writing – review & editing, Supervision. **Doekle R. Yntema:** Writing – review & editing, Supervision. **Rob G.H. Lammertink:** Methodology, Conceptualization, Writing – review & editing, Supervision.

Declaration of competing interest

The authors declare that they have no known competing financial interests or personal relationships that could have appeared to influence the work reported in this paper.

Data availability

Data will be made public after acceptance of paper via 4TU.data.

Acknowledgments

This work was performed in the cooperation framework of Wetsus, European Centre of Excellence for Sustainable Water Technology, The Netherlands (www.wetsus.nl). Wetsus is cofunded by the Dutch Ministry of Economic Affairs and Ministry of Infrastructure and Environment, the European Union Regional Development Fund, the Province of Fryslân, and the Norther Netherlands Provinces. This work is part of a project that has received funding from the European Union's Horizon 2020 research and innovation program under the Marie Skłodowska-Curie grant agreement 665874. The authors thank the participants of the research theme "Priority compounds and Virus control" for fruitful discussions and financial support. The authors would also like to thank Nikos Kyriakou and Farzaneh Radmanesh for the help with the preparation of the membranes, Eva Portillo for her assistance in the experiments, Marianne Heegstra and Ineke Punt with the aid with the

SEM pictures, and Pim Bullee, Niels Hakkert and Max Kwak for their collaboration in Matlab. All authors have approved the final article.

References

[1] R. Baker, Membrane Technology and Applications, John Wiley & Sons, Ltd. Publication, The Atrium, 2012, http://dx.doi.org/10.1016/S0958-2118(96)90133-0.

[2] J.M. Poyatos, M.M. Muñio, M.C. Almecija, J.C. Torres, E. Hontoria, F. Osorio, Advanced oxidation processes for wastewater treatment: State of the art, Water Air Soil Pollut. 205 (1) (2009) 187, http://dx.doi.org/10.1007/s11270-009-0065-1.

[3] A. Fujishima, T.N. Rao, D.A. Tryk, Titanium dioxide photocatalysis, J. Photochem. Photobiol. C Photochem. Rev. 1 (1) (2000) 1–21, http://dx.doi.org/10.1016/S1389-5567(00)00002-2.

[4] S.M. Samaei, S. Gato-Trinidad, A. Altaee, The application of pressure-driven ceramic membrane technology for the treatment of industrial wastewaters—A review, Separation Purif. Technol. 200 (2018) 198–220, http://dx.doi.org/10.1016/j.seppur.2018.02.041.

[5] T. Yang, F. Liu, H. Xiong, Q. Yang, F. Chen, C. Zhan, Fouling process and anti-fouling mechanisms of dynamic membrane assisted by photocatalytic oxidation under sub-critical fluxes, Chin. J. Chem. Eng. 27 (8) (2019) 1798–1806, http://dx.doi.org/10.1016/j.cjche.2018.10.019.

[6] L.T. Nyamutswa, B. Zhu, S.F. Collins, D. Navaratna, M.C. Duke, Light conducting photocatalytic membrane for chemical—free fouling control in water treatment, J. Membr. Sci. 604 (2020) 118018, http://dx.doi.org/10.1016/j.memsci.2020.118018.

[7] N. Nasrollahi, L. Ghalamchi, V. Vatanpour, A. Khataee, Photocatalytic-membrane technology: a critical review for membrane fouling mitigation, J. Ind. Eng. Chem. 93 (2021) 101–116, http://dx.doi.org/10.1016/j.jiec.2020.09.031.

[8] T. Van Gestel, H. Kruidhof, D.H. Blank, H.J. Bouwmeester, ZrO_2 And TiO_2 membranes for nanofiltration and pervaporation: Part 1. Preparation and characterization of a corrosion-resistant ZrO_2 nanofiltration membrane with a MWCO<300, J. Membr. Sci. 284 (1) (2006) 128–136, http://dx.doi.org/10.1016/j.memsci.2006.07.020.

[9] M.E. Leblebici, G.D. Stefanidis, T. Van Gerven, Comparison of photocatalytic space–time yields of 12 reactor designs for wastewater treatment, Chem. Eng. Process. Process Intensif. 97 (2015) 106–111, http://dx.doi.org/10.1016/j.cep.2015.09.009.

[10] C. Casado, R. Timmers, A. Sergejevs, C. Clarke, D. Allsopp, C. Bowen, R. van Grieken, J. Marugán, Design and validation of a led-based high intensity photocatalytic reactor for quantifying activity measurements, Chem. Eng. J. 327 (2017) 1043–1055, http://dx.doi.org/10.1016/j.cej.2017.06.167.

[11] R.B.P. Marcelino, C.C. Amorim, Towards visible-light photocatalysis for environmental applications: band-gap engineering versus photons absorption—a review, Environ. Sci. Pollut. Res. 26 (5) (2019) 4155–4170, http://dx.doi.org/10.1007/s11356-018-3117-5.

[12] D. Rafieian, R.T. Driessen, W. Ogieglo, R.G.H. Lammertink, Intrinsic photocatalytic assessment of reactively sputtered TiO_2 films, ACS Appl. Mater. Interfaces 7 (16) (2015) 8727–8732, http://dx.doi.org/10.1021/acsami.5b01047.

[13] I. Dundar, A. Mere, V. Mikli, M. Krunks, I. Oja Acik, Thickness effect on photocatalytic activity of TiO_2 thin films fabricated by ultrasonic spray pyrolysis, Catalysts 10 (9) (2020) http://dx.doi.org/10.3390/catal10091058.

[14] A. Visan, D. Rafieian, W. Ogieglo, R.G.H. Lammertink, Modeling intrinsic kinetics in immobilized photocatalytic microreactors, Appl. Catal. B 150–151 (2014) 93–100, http://dx.doi.org/10.1016/j.apcatb.2013.12.003.

[15] I. Horovitz, D. Avisar, M.A. Baker, R. Grilli, L. Lozzi, D. Di Camillo, H. Mamane, Carbamazepine degradation using a N–doped TiO2 coated photocatalytic membrane reactor: Influence of physical parameters, J. Hard Mater. 310 (2016) 98–107, http://dx.doi.org/10.1016/j.jhazmat.2016.02.008.

[16] D.D. Phan, F. Babick, M.T. Nguyen, B. Wessely, M. Stintz, Modelling the influence of mass transfer on fixed-bed photocatalytic membrane reactors, Chem. Eng. Sci. 173 (2017) 242–252, http://dx.doi.org/10.1016/j.ces.2017.07.043.

[17] W. Li, A. Elzatahry, D. Aldhayan, D. Zhao, Core—shell structured titanium dioxide nanomaterials for solar energy utilization, Chem. Soc. Rev. 47 (2018) 8203–8237, http://dx.doi.org/10.1039/C8CS00443A.

[18] R.K. Herz, Intrinsic kinetics of first-order reactions in photocatalytic membranes and layers, Chem. Eng. J. 99 (3) (2004) 237–245, http://dx.doi.org/10.1016/j.cej.2003.11.013.

[19] D.F. Ollis, Integrating photocatalysis and membrane technologies for water treatment, Ann. New York Acad. Sci. 984 (1) (2003) 65–84, http://dx.doi.org/10.1111/j.1749-6632.2003.tb05993.x.

[20] S.A. Heredia Deba, B.A. Wols, D.R. Yntema, R.G.H. Lammertink, Transport and surface reaction model of a photocatalytic membrane during the radical filtration of methylene blue, Chem. Eng. Sci. 254 (2022) 117617, http://dx.doi.org/10.1016/j.ces.2022.117617.

[21] R.J.R. Uhlhorn, M.H.B.J. Huis In't Veld, K. Keizer, A.J. Burggraaf, Synthesis of ceramic membranes, J. Mater. Sci. 27 (2) (1998) 527–537, http://dx.doi.org/10.1007/BF00543947.

[22] M. ten Hove, M.W. Luiten-Olieman, C. Huiskes, A. Nijmeijer, L. Winnubst, Hydrothermal stability of silica, hybrid silica and zr-doped hybrid silica membranes, Separation Purif. Technol. 189 (2017) 48–53, http://dx.doi.org/10.1016/j.seppur.2017.07.045.

[23] S. Abedini, N. Parvin, P. Ashtari, F.S. Jazi, Microstructure, strength and CO_2 separation characteristics of α-alumina supported γ-alumina thin film membrane, Adv. Appl. Ceram. 112 (1) (2013) 17–22, http://dx.doi.org/10.1179/1743676112Y.0000000043.

[24] F. Cuperus, D. Bargeman, C. Smolders, Permporometry: the determination of the size distribution of active pores in UF membranes, J. Membr. Sci. 71 (1–2) (1992) 57–67, http://dx.doi.org/10.1016/0376-7388(92)85006-5.

[25] A. Fujishima, K. Honda, Electrochemical photolysis of water at a semiconductor electrode, Nature 238 (5358) (1972) 37–38, http://dx.doi.org/10.1038/238037a0.

[26] I. Izumi, W.W. Dunn, K.O. Wilbourn, F.-R.F. Fan, A.J. Bard, Heterogeneous photocatalytic oxidation of hydrocarbons on platinized titanium dioxide powders, J. Phys. Chem. 84 (24) (1980) 3207–3210, http://dx.doi.org/10.1021/j100461a015.

[27] S.A. Heredia Deba, B.A. Wols, D.R. Yntema, R.G.H. Lammertink, Effects of the water matrix on the degradation of micropollutants by a photocatalytic ceramic membrane, Membranes 12 (10) (2022) http://dx.doi.org/10.3390/membranes12101004.

[28] P. Danckwerts, Continuous flow systems: Distribution of residence times, Chem. Eng. Sci. 2 (1) (1953) 1–13, http://dx.doi.org/10.1016/0009-2509(53)80001-1.

[29] M. Aguado, M. Anderson, C. Hill, Influence of light intensity and membrane properties on the photocatalytic degradation of formic acid over TiO_2 ceramic membranes, J. Mol. Catal. 89 (1) (1994) 165–178, http://dx.doi.org/10.1016/0304-5102(93)E0282-L.

[30] C. Brinker, A. Hurd, P. Schunk, G. Frye, C. Ashley, Review of sol–gel thin film formation, J. Non-Cryst. Solids 147–148 (1992) 424–436, http://dx.doi.org/10.1016/S0022-3093(05)80653-2.

[31] C. Brinker, G.W. Scherer, Sol-Gel Science, Academic Press, San Diego, 1990.

[32] Q. Fan, B. McQuillin, A.K. Ray, M.L. Turner, A.B. Seddon, High density, non—porous anatase titania thin films for device applications, J. Phys. D: Appl. Phys. 33 (21) (2000) 2683–2686, http://dx.doi.org/10.1088/0022-3727/33/21/303.

[33] A. Alem, H. Sarpoolaky, M. Keshmiri, Sol—gel preparation of titania multilayer membrane for photocatalytic applications, Ceram. Int. 35 (5) (2009) 1837–1843, http://dx.doi.org/10.1016/j.ceramint.2008.10.034.

[34] S.A. Heredia Deba, B.A. Wols, D.R. Yntema, R.G. Lammertink, Photocatalytic ceramic membrane: Effect of the illumination intensity and distribution, J. Photochem. Photobiol. A 437 (2023) 114469, http://dx.doi.org/10.1016/j.jphotochem.2022.114469.

[35] S. Lizhong, J.R. Bolton, Determination of the quantum yield for the photochemical generation of hydroxyl radicals in TiO_2 suspensions, J. Phys. Chem. 100 (1996) 4127–4134.

[36] S.K. Loeb, P.J.J. Alvarez, J.A. Brame, E.L. Cates, W. Choi, J. Crittenden, D.D. Dionysiou, Q. Li, G. Li-Puma, X. Quan, D.L. Sedlak, T. David Waite, P. Westerhoff, J.-H. Kim, The technology horizon for photocatalytic water treatment: Sunrise or sunset? Environ. Sci. Technol. 53 (6) (2019) 2937–2947, http://dx.doi.org/10.1021/acs.est.8b05041.

[37] R.W. Matthews, Photocatalytic oxidation and adsorption of methylene blue on thin films of near-ultraviolet-illuminated TiO_2, J. Chem. Soc. Faraday Trans. I 85 (6) (1989) 1291–1302, http://dx.doi.org/10.1039/F19898501291.

[38] J. Tschirch, R. Dillert, D. Bahnemann, Photocatalytic degradation of methylene blue on fixed powder layers: Which limitations are to be considered? J. Adv. Oxid. Technol. 11 (2) (2008) 193–198, http://dx.doi.org/10.1515/jaots-2008-0202.

[39] J. Tschirch, R. Dillert, D. Bahnemann, B. Proft, A. Biedermann, B. Goer, Photodegradation of methylene blue in water, a standard method to determine the activity of photocatalytic coatings? Res. Chem. Intermed. 34 (4) (2008) 381–392, http://dx.doi.org/10.1163/156856708784040588.

[40] Q. Zhang, C. Li, T. Li, Rapid photocatalytic degradation of methylene blue under high photon flux UV irradiation: Characteristics and comparison with routine low photon flux, Int. J. Photoenergy 2012 (2012) 398787, http://dx.doi.org/10.1155/2012/398787.

[41] T.A. Egerton, The influence of surface alumina and silica on the photocatalytic degradation of organic pollutants, Catalysts 3 (1) (2013) 338–362, http://dx.doi.org/10.3390/catal3010338.

[42] C.M. Gómez, G.D. Angel, E. Ramos-Ramírez, I. Rangel-Vázquez, F. González, A. Arrieta, A. Vázquez-Zavala, A. Bonilla-Sánchez, M. Sánchez Cantú, Alumina coating with TiO2 and its effect on catalytic photodegradation of phenol and p-cresol, J. Chem. Technol. Biotechnol. 91 (8) (2016) 2211–2220, http://dx.doi.org/10.1002/jctb.5025.